

UCLA

UCLA Previously Published Works

Title

Observational evidence for active dust storms on Titan at equinox

Permalink

<https://escholarship.org/uc/item/3f2657tr>

Journal

Nature Geoscience, 11(10)

ISSN

1752-0894

Authors

Rodriguez, S
Le Mouélic, S
Barnes, JW
[et al.](#)

Publication Date

2018-10-01

DOI

10.1038/s41561-018-0233-2

Peer reviewed

1 **Observational evidence for active dust storms on Titan at equinox**

2 S. Rodriguez^{1*}, S. Le Mouélic², J. W. Barnes³, J. F. Kok⁴, S. C. R. Rafkin⁵, R. D. Lorenz⁶, B.
3 Charnay⁷, J. Radebaugh⁸, C. Nartea¹, T. Cornet⁹, O. Bourgeois², A. Lucas¹, P. Rannou¹⁰, C. A.
4 Griffith¹¹, A. Coustenis⁷, T. Appéré¹², M. Hirtzig^{7†}, C. Sotin¹³, J. M. Soderblom¹⁴, R. H.
5 Brown¹¹, J. Bow³, G. Vixie³, L. Maltagliati^{1††}, S. Courrech du Pont¹⁵, R. Jaumann¹⁶, K.
6 Stephan¹⁶, K. H. Baines¹⁷, B. J. Buratti¹³, R. N. Clark¹⁸, P. D. Nicholson¹⁹

7 ¹Institut de Physique du Globe de Paris, Sorbonne Paris Cité, Univ Paris Diderot, UMR 7154
8 CNRS, 1 rue Jussieu, 75238 Paris, Cedex 05, France.

9 ²Laboratoire de Planétologie et Géodynamique (LPGNantes), CNRS-UMR 6112, Université de
10 Nantes, 44322 Nantes, France.

11 ³University of Idaho, Department of Physics, 875 Perimeter Drive MS0903, Moscow, ID 83844-
12 0903, USA.

13 ⁴Department of Atmospheric and Oceanic Sciences, University of California, Los Angeles,
14 California, USA.

15 ⁵Planetary Atmospheres and Surfaces, Department of Space Studies, Southwest Research
16 Institute, Boulder, Colorado 80302, USA.

17 ⁶Johns Hopkins University Applied Physics Laboratory, Laurel, Maryland, USA.

18 ⁷ LESIA, Observatoire de Paris, PSL-Research Univ., CNRS, Univ. Pierre et Marie Curie Paris
19 06, Sorbonne Univ., Univ. Paris-Diderot, Sorbonne Paris-Cité, 5, place Jules Janssen, 92195
20 Meudon Cedex, France.

21 ⁸Department of Geological Sciences, Brigham Young University, Provo, UT 84602, USA.

22 ⁸Institut de Physique du Globe de Paris, Sorbonne Paris Cité, Univ Paris Diderot, UMR 7154
23 CNRS, 1 rue Jussieu, 75238 Paris, Cedex 05, France.

24 ⁹European Space Agency (ESA), European Space Astronomy Centre (ESAC), Villanueva de la
25 Canada, Spain.

26 ¹⁰Groupe de Spectroscopie Moléculaire et Atmosphérique, UMR CNRS 6089, Université de
27 Reims, U.F.R. Sciences Exactes et Naturelles, Moulin de la Housse B.P. 1039, 51687 Reims
28 Cedex 2, France.

29 ¹¹Department of Planetary Sciences, University of Arizona, Lunar and Planetary Laboratory,
30 1629 E. University Blvd., Tucson, AZ 85721, USA.

31 ¹²Institut de Planétologie et d'Astrophysique de Grenoble, Université J. Fourier, CNRS/INSU,
32 Grenoble, France.

33 ¹³California Institute of Technology/Jet Propulsion Laboratory, 4800 Oak Grove Drive,
34 Pasadena, CA 91109, USA.

35 ¹⁴Department of Earth, Atmospheric, and Planetary Sciences, Massachusetts Institute of
36 Technology, Cambridge, MA 02139, USA.

37 ¹⁵Laboratoire Matière et Systèmes Complexes, Université Paris Diderot, Paris, France.

38 ¹⁶German Aerospace Centre (DLR), Institute of Planetary Research, 12489 Berlin, Germany.

39 ¹⁷Space Science and Engineering Center, University of Wisconsin, Madison, WI 53706, USA.

40 ¹⁸Planetary Science Institute, 1700 East Fort Lowell, Suite 106, Tucson, AZ 85719, USA.

41 ¹⁹Department of Astronomy, Cornell University, Ithaca, New York, USA.

42 *Correspondence to: sebastien.rodriquez@cea.fr

43 †Current address: Fondation ‘‘La main à la pâte’’, Montrouge, France.

44 ††Current address: Springer Nature, London, UK.

45

46

47

48

49

50

51

52

53

54

55

56

57

58

59

60

61

62 **Abstract:** [230 words]

63 **Saturn's moon Titan has a dense nitrogen-rich atmosphere with methane as its primary**
64 **volatile. Titan's atmosphere experiences an active chemistry that produces a haze of**
65 **organic aerosols that settle to the surface and a dynamic climate in which hydrocarbons are**
66 **cycled between clouds, rain and seas. Titan's displays particularly energetic meteorology at**
67 **equinox in equatorial regions, including sporadic and large methane storms. In 2009, near**
68 **Titan's northern spring equinox, the Cassini spacecraft observed three distinctive and**
69 **short-lived spectral brightenings close to the equator. Here we show from analyses of**
70 **Cassini spectral data, radiative transfer modelling, and atmospheric simulations that the**
71 **brightenings originate in the atmosphere and are consistent with formation from dust**
72 **storms composed of micron-sized solid organic particles mobilized from underlying dune**
73 **fields. Although the Huygens lander found evidence that dust can be kicked up locally from**
74 **Titan's surface, our findings suggest that dust can be suspended in Titan's atmosphere at**
75 **much larger spatial scale. Mobilization of dust and injection into the atmosphere would**
76 **require dry conditions and unusually strong near-surface winds (about 5 times more than**
77 **estimated ambient winds). Such strong winds are expected to occur in downbursts during**
78 **rare equinoctial methane storms - consistent with the timing of the observed brightenings.**
79 **Our findings imply that Titan – like Earth and Mars – has an active dust cycle, which**
80 **suggests that Titan's dune fields are actively evolving by aeolian processes.**

81

82 **Main Text:** [2725 words]

83 Along with Earth-based surveys, the close and frequent observations of Titan by the
84 Cassini spacecraft, in orbit around Saturn since July 2004, allowed us to see down to Titan's

85 surface and uncover evidence that the lowest part of its thick atmosphere experiences an exotic
86 meteorological cycle analogous to Earth's hydrological cycle, involving methane evaporation,
87 condensation into clouds¹⁻⁵, and rainfall^{1,5,6}. Long-term monitoring campaigns have revealed that
88 Titan's cloud coverage varies significantly with latitude and season¹⁻⁴. General Circulation
89 Models (GCMs) have suggested that the observed varying distribution of clouds is a natural
90 consequence of the seasonally changing pattern of global atmospheric circulation^{1-4,7-11}. This
91 results in a net transport of methane from the tropics to the poles, drying the equatorial regions⁷⁻
92 ¹¹. Titan's surface bears the marks of such climatic forcing through the presence of extensive and
93 numerous liquid reservoirs and sustained cloud activity near the poles¹⁻⁴, and more arid
94 conditions at equator, with intense, but relatively scarce meteorological activity^{3-5,12,13} and
95 widespread dune fields^{14,15}.

96 Indeed, only a few tropospheric clouds have been observed in Titan's equatorial regions¹⁻
97 ^{5,12,13}. Very close to spring equinox (August 2009), with a more direct solar illumination of the
98 equatorial regions, clouds occurred near the equator a little more frequently and appeared to
99 grow in size and energy, counting three major events in April 2008, September and October
100 2010^{5,12}. This increase in cloud activity indicates that a very active equinoctial meteorology
101 occurs in the equatorial regions, confirming GCM predictions during this short time interval⁸⁻¹¹.
102 Here we show new Cassini observations that illustrate the energetic meteorological conditions
103 that prevail near Titan's equator during equinoxes and their possible impact on geomorphic
104 processes.

105

106 **Infrared equatorial brightenings at equinox**

107

108 We report here singular and transient changes on Titan in the form of diffuse bright spots
109 of unusual infrared color, that were detected by the Visual and Infrared Mapping Spectrometer
110 (VIMS)¹⁶ onboard Cassini. **Figure 1 and 2** show VIMS images and spectra of the only three
111 events of this kind detected so far. They were observed during Titan flybys T56 (22 May 2009 –
112 Titan solar longitude $L_s = 357.9^\circ$), T65 (13 January 2010 – $L_s = 5.3^\circ$) and T70 (21 June 2010 –
113 $L_s = 10.7^\circ$), all near in time to Titan’s northern spring equinox ($L_s = 0^\circ$ by definition) (**Fig. S1a**).
114 These observations revealed an intense and short-lived infrared brightening of large regions
115 usually dark, very close to the equator. These brightenings lasted at least 11 to 14 hours (time
116 during which the brightened areas are visible from Cassini orbit), but no more than 4 to 5
117 terrestrial weeks (less than three Titan days), since they only appeared in one flyby, except for
118 the T70 event possibly still observable at T71 (7 July 2010). The three bright spots cover large
119 areas, systematically over dune fields ($\approx 420\,000\text{ km}^2$ over Senkyo, $\approx 250\,000\text{ km}^2$ over Belet and
120 $\approx 180\,000\text{ km}^2$ over Shangri-La for the T56, T65 and T70 events respectively – **Fig. 1 and S1b**)
121 and present a somewhat elongated shape in the zonal direction. Spectrally, these bright spots are
122 observed only at the center and near-wings of the infrared atmospheric windows, suggesting
123 surface or very low atmospheric features (**Fig. S2**). Their near-infrared (0.88-5.1 μm) spectra all
124 present a pronounced positive slope (**Fig. 2**). They are brighter than the surrounding surface at
125 wavelengths greater than 1.6- μm , particularly at 5- μm , and start dimming below 1.6- μm , fading
126 almost totally at 0.93- μm , thus undetectable with the Imaging Science Subsystem (ISS) cameras
127 onboard Cassini (**Fig. S3**). Note that the affected areas have similar spectra before and after the
128 ephemeral brightening events (**Fig. 2**). The spectral characteristics of these brightenings differ
129 significantly from those of all known examples of surface and atmospheric brightenings, such as
130 tropospheric clouds or deposition of frost onto the surface (**Fig. S3**), which are bright and

131 detectable in all near-infrared windows^{2,3,6}, revealing a substantial difference in nature
132 (composition and/or altitude) and origin.

133

134 **Evidence for large storms of organic dust**

135

136 We investigate different possible explanations for these singular brightening events,
137 considering both surface and atmospheric phenomena.

138 Given the particularly high brightness of these regions at 5- μm , we first examine the
139 possibility of localized cryovolcanic hot spots. Considering that hypothetical eruptions on Titan
140 are more likely effusive than explosive¹⁷, the sudden apparition of these bright (hot?) spots over
141 extensive areas is however hardly compatible with the slow outpouring and spreading of viscous
142 lava flows. The timescale at which the T56, T65 and T70 events vanish is also difficult to
143 reconcile with the timescale of cryolava cooling back to the average surface temperature of
144 Titan, which has been calculated to be 1 to 2 orders of magnitude longer (≈ 100 to 1000 terrestrial
145 days depending on the lava composition¹⁸) than the observed durations. Finally, calculations of
146 the thermal emission of a hot surface (with temperatures ranging from 100 to 250 K) show that
147 no temperature can satisfactorily explain the spectral slope observed between 1.6 and 5- μm for
148 the three events (**Fig. S5**). Lava flows would also induce lasting surface changes, which are not
149 observed.

150 Surface brightenings could be provoked by methane precipitation and subsequent
151 freezing at the surface^{5,6}. Such events have been reported by ISS and VIMS instruments in the
152 wake of the 2010 September giant cloudburst⁶ at roughly the same epoch and latitudes as the
153 T56, T60 and T70 events. However, these precipitation-induced brightenings are characterized

154 by an evolution timescale of several terrestrial months and a rise in flux in all atmospheric
155 windows⁶ (see an example in **Fig. S3**). None of the T56, T60 and T70 bright spots match those
156 characteristics.

157 Finally, we explore the possibility that these local rises in brightness may have an
158 atmospheric origin. To that end, we apply a radiative transfer model that simulates the scattering
159 and absorption of sunlight by Titan’s atmosphere, producing synthetic spectra for comparison
160 with the observations.

161 Our radiative transfer model is an updated version of the model presented in detail in (ref.
162 *19* and references therein), using the same atmospheric databases (haze and gases) and a similar
163 methodology to derive haze optical depth and surface albedo (ref. *19* and Supplementary
164 Information). The main novelty concerns the possibility to simulate an additional “cloud” layer
165 composed of spherical particles in the lowest part of the atmosphere. This cloud is characterized
166 by four parameters: top altitude, optical depth, particle effective radius and composition (either
167 liquid methane or tholin-like organics analogous to airborne Titan’s haze particles, presumably
168 the main contributor to dune material composition^{15, 19-24}).

169 We first retrieved “before” and “after” surface albedos at the same location as the T56,
170 T65 and T70 bright spots from flybys closely bracketing them in time (see **Fig. 1 and 2**). As the
171 surface is clearly visible in those observations, we perform the radiative transfer calculations
172 without the additional cloud layer. The striking similarity of the “before” and “after” surface
173 albedos at all wavelengths (**Fig. S4**) tells us that the brightening events have not substantially
174 changed the properties of the surface.

175 These surface albedos were then used as inputs to model the “event” spectra extracted
176 from the central and brightest pixel of the T56, T65 and T70 bright spots (**Fig. 2**). The “surface-

177 only” model was unable to reproduce any of the event spectra, especially the high reflectance
178 above 1.6- μm (**Fig. 3**). No enhancement in the local population of fractal aerosols or low altitude
179 mist, both too dark in the infrared^{19,25}, especially at wavelengths greater than 2- μm ¹⁹, can better
180 explain the observed spectra. We therefore searched for the best fits between observed and
181 simulated spectra by adding a low altitude cloud, for various opacities, particle sizes, top
182 altitudes and compositions. The inversions have been performed by using a **combination of**
183 **Genetic and** Levenberg-Marquardt algorithms (Supplementary Information).

184 In all cases, the best fits to the observed spectra over the full VIMS infrared range are
185 provided by the addition of a cloud of solid organic particles. Those tholin-like clouds are found
186 to be optically thin, with opacity ~ 0.5 , composed of small particles (~ 5 microns in diameter), and
187 confined at low altitude, with a maximum top altitude of ~ 10 -14 km (**Fig. 3 and Table S5**).

188 We cannot completely exclude liquid methane clouds, despite systematic poorer fits, on
189 the sole basis of fitting statistics (**Fig. 3 and Table S5**). However, the best retrieved parameters
190 for methane clouds all point to unusually low top altitudes (10-13 km) and small droplet size (~ 5
191 microns), casting some doubts on the possibility of their physical existence. Cloud simulations
192 using the TRAMS model^{26,27} were therefore conducted at the time and location of the observed
193 brightenings, in order to further investigate both methane convective and stratiform clouds as
194 **possible** explanations. The details and results of the **cloud** modelling studies are thoroughly
195 discussed in the Supplementary Information. The radiative transfer modeling found that methane
196 clouds, if real, should be restricted to altitudes below ≈ 13 km and probably lower (**Fig. 3 and**
197 **Table S5**). At the season and location where the brightenings are observed, thermodynamics
198 **suggest** that any methane clouds with a base below this level would be necessarily convective in
199 nature and would extend to much greater altitudes. Depending on the relative humidity of Titan’s

200 surface, the top altitude of such a convective cloud would reach at minimum 25 km. Moreover,
201 we also calculated the microphysical properties (droplet size distribution and number density) of
202 such clouds with the TRAMS model, still under the temperature and wind conditions at the
203 equator and for the spring equinox, and it turns out that they are also completely inconsistent
204 with the radiative transfer retrievals by several orders of magnitude. **TRAMS simulations lead**
205 **indeed** to significantly optically thicker clouds than those possibly observed with VIMS **and**
206 **considered in this study**. On their side, stratiform clouds below ≈ 13 km are not physically
207 possible given the thermodynamic sounding. Stratiform clouds above 13 km may be possible,
208 but they would be shallow and also inconsistent with the physical properties of the retrieved
209 clouds. For all these reasons, methane clouds, either convective or stratiform, as retrieved by the
210 radiative transfer modelling, are simply unphysical and must be rejected.

211 Gathering together all of the observations, including locations, directly above giant sand
212 seas, timing, close to spring equinox when the strongest winds are expected to episodically blow,
213 spectral characteristics, pointing to solid organics equivalent to the material constituting the
214 dunes, and cloud dynamics, we conclude that the best, and only remaining explanation for these
215 three bright spots **may be** short-lived dust storms composed of fine organic particles, smaller
216 than sand-sized particles, lifted from the underlying dune fields.

217

218 **Implication for equatorial near-surface winds at equinoxes**

219

220 At local scale, it has already been demonstrated not only that dust **is likely to** exist on the
221 surface of Titan, but also that winds less than 5 m/s **may** lift it: the penetrometer of the Huygens
222 probe which landed near Titan's equator in 2005 indicated an uppermost thin (few mm) layer of

223 soft/low-density material²⁸, and optical measurements showed dust around the probe for 2-4
224 seconds after impact²⁹. This dust was **most possibly** lifted by the turbulent aerodynamic wake of
225 the probe^{29,30}, which landed at 5.4 m/s. In our case, the **possibility for** large scale storms of dust
226 has more significant implications for the atmospheric dynamics and sedimentology of the moon.

227 In order to investigate the possible onset of dust storms on Titan, we adapted models of
228 sediment transport that were initially developed for Earth, Mars and Venus³¹⁻³³ to Titan's near-
229 surface conditions. These models, based on semi-empirical or analytical calculations, allow us to
230 predict the minimum friction velocity needed to initiate and sustain sediment transport (**Fig. 4**
231 and Supplementary Information).

232 Dust can be emitted through three primary processes³⁴: (i) direct aerodynamic lifting, (ii)
233 indirect ejection from the surface by impacts of saltating sand particles, or (iii) lifting of sand-
234 sized aggregates of dust particles that fragment upon impact on the surface. Our radiative
235 transfer modelling points to particles in suspension with a diameter of ~5 microns. Aerodynamic
236 lifting of such small particles, that experience large cohesive forces, requires a minimum friction
237 velocity as high as 0.1 to 0.5 m/s (**Fig. 3**). Using the classical Karman's logarithmic wind
238 velocity profile with a rugosity length of 5 mm, those friction velocities correspond to a wind
239 blowing at ~2.5 to 11 m/s at 40 m altitude. Dust emission through saltation of sand particles
240 (with an optimal size of 300 microns) would have a lower threshold friction velocity for lifting
241 (~0.06 m/s) than that for dust (**Fig. 3**), requiring wind speed of ~1.4 m/s at 40 m altitude.
242 However, compared to Earth and Mars, the lower gravity and higher fluid density on Titan
243 substantially reduces the energy with which saltating particles impact the surface³⁴. This implies
244 that dust emission through saltator bombardment **may be** less efficient than it is on Earth and
245 Mars (**Fig. S10**). Dust could also be emitted through the formation³⁵, lifting and fragmentation at

246 impact of sand-sized aggregates of dust. Owing to their lower density, **such aggregates could**
247 **present a threshold for lifting slightly below 1.4 m/s and be** more easily lifted than dust and
248 sand particles³⁴. Dust emission through this process would not necessarily involve active sand
249 transport, an effect that has been observed directly on Mars³⁶. In any case, micron-sized dust
250 emission is systematically accompanied by the mobilization of larger particles, more easily
251 unstuck from surface (**Fig. 4**). **Since** larger particles have higher fall velocity and will settle
252 down rapidly, **they generally stay** confined close to the surface, while smaller particles can rise
253 to higher altitudes and remain suspended for much longer time, generating the observed dust
254 cloud. This is what can be observed on terrestrial and **Martian** dust storms and this can explain
255 why the dust clouds we report here are dominated by the infrared signature of micron-sized
256 particles.

257 Regardless of the process, dust injection into the atmosphere requires near-surface winds
258 much stronger than the ambient averaged winds predicted to blow during equinoxes (maximum
259 of ~0.3 m/s at 40 m altitude (e.g. ref 10)). Only gusts, either appearing when considering wind
260 statistics at high temporal frequency (i.e. capturing the turbulence associated with the equinoctial
261 passage of the intertropical convergence zone³⁷) or produced ahead of rare, but large methane
262 storms, as simulated in mesoscale methane cloud models^{38,39}, can exceed 1 m/s at 40 m altitude
263 and even reach 10 m/s for a few hours for the methane storms^{38,39}. In both cases, gusts have the
264 highest probability to occur during equinox in the equatorial regions, precisely when and where
265 we **possibly** observe the dust storms. A few large equatorial storms have been observed very
266 close to the equinox^{5,12} (**Fig. S1a**). The most energetic of these **may** constitute the best, and
267 timely, candidates for generating surface winds strong enough to inject organic dust into Titan's
268 air (this mechanism would thus be analogous to Earth's "haboobs"). Their uncommonness **may**

269 further explain the rareness of dust storm detections by Cassini. Such equatorial storms are also
270 thought to sustain active sediment transport over the dunes and control their growth and
271 orientation³⁸.

272 No equatorial methane storms have been yet detected preceding closely any of the T56,
273 T65 and T70 events. But given the frequency of Cassini flybys of Titan (one per month in
274 average) and the relative short living of methane storms (only a few to a few tens of hours), it is
275 quite likely that those precursors have been missed and that we were only able to see the
276 succeeding, and more persistent, dust cloud. In a same manner, no dust storms have been seen by
277 Cassini after the gigantic methane storms observed in Titan's equatorial regions in October 2010
278 (ref. 5), but the fact that Cassini flew back by Titan only four months later may explain that, in
279 that case, no dust storm could have been triggered or that we may have missed this event, if any.

280 The requirement of strong near-surface winds implies that dust lifting can be
281 accompanied by saltation of the underlying dune sand. This constitutes additional clues for sand-
282 saltating winds within currently active dune fields. This may only occur at equinoxes, every 14.7
283 terrestrial years. Besides the Earth and Mars, Titan would thus be the only other body in the
284 Solar System where dust storms and aeolian activity over dune fields have been observed,
285 indicating the complexity of the atmospheric dynamics and atmosphere-surface interactions at
286 play on Saturn's largest moon. The dust storms may also indicate an ongoing participation for
287 dust within Titan's global organic cycle³⁵.

288

289 **Data sources.** VIMS data are available via NASA's Planetary Data System (PDS):

290 http://pds-atmospheres.nmsu.edu/data_and_services/atmospheres_data/Cassini/vims.html.

291

292 **Data availability.** The data that supports the analysis and plots within this paper and other
293 findings of this study are available from the corresponding author upon request.

294

295 **References:**

296 1. E. P. Turtle *et al.*, 2009, Cassini imaging of Titan’s high-latitude lakes, clouds, and south-
297 polar surface changes. *Geophys. Res. Lett.* **36**, L2204 (2009).

298 2. S. Rodriguez *et al.*, Global circulation as the main source of cloud activity on Titan. *Nature*
299 **459**, 678–682 (2009).

300 3. S. Rodriguez *et al.*, Titan’s cloud seasonal activity from winter to spring with Cassini/VIMS.
301 *Icarus* **216**, 89–110 (2011).

302 4. E. P. Turtle *et al.*, Seasonal changes in Titan’s meteorology. *Geophys. Res. Lett.* **38**, L03203
303 (2011).

304 5. E. P. Turtle *et al.*, Rapid and extensive surface changes near Titan’s equator: Evidence of
305 April showers. *Science* **331**, 1414–1417 (2011).

306 6. J. W. Barnes *et al.*, Precipitation-induced surface brightenings seen on Titan by Cassini VIMS
307 and ISS. *Planet. Sci.* **2**, 1 (2013).

308 7. P. Rannou, F. Montmessin, F. Hourdin, S. Lebonnois, S., The latitudinal distribution of clouds
309 on Titan. *Science* **311**, 201–205 (2006).

310 8. J. L. Mitchell, The drying of Titan’s dunes: Titan’s methane hydrology and its impact on
311 atmospheric circulation. *J. Geophys. Res.* **113**, E08015 (2008).

312 9. T. Schneider, S. D. B. Graves, E. L. Schaller, M. E. Brown, Polar methane accumulation and
313 rainstorms on Titan from simulations of the methane cycle. *Nature* **481**, 58–61 (2012).

- 314 10. J. M. Lora, J. I. Lunine, J. L. Russell, GCM simulations of Titan's middle and lower
315 atmosphere and comparison to observations. *Icarus* **250**, 516-528 (2015).
- 316 11. J. L. Mitchell and J. M. Lora, The climate of Titan. *AREPS* **44**, 353-380 (2016).
- 317 12. E. L. Schaller, H. G. Roe, T. Schneider, M. E. Brown, Storms in the tropics of Titan. *Nature*
318 **460**, 873-875 (2009).
- 319 13. C. A. Griffith et al., Characterization of clouds in Titan's tropical atmosphere. *Astrophys. J.*
320 **702**, L105–L109 (2009).
- 321 14. R. D. Lorenz *et al.*, The sand seas of Titan: Cassini RADAR observations of longitudinal
322 dunes, *Science* **312**, 724-727 (2006).
- 323 15. S. Rodriguez *et al.*, Global mapping and characterization of Titan's dune fields with Cassini:
324 Correlation between RADAR and VIMS observations. *Icarus* **230**, 168-179 (2014).
- 325 16. R. H. Brown *et al.*, The Cassini Visual and Infrared Mapping Spectrometer investigation.
326 *Space Sci. Rev.* **115**, 111–168 (2004).
- 327 17. R. D. Lorenz, Pillow lava on Titan: expectations and constraints on cryovolcanic processes.
328 *Planet. Space Sci.* **44**, 1021-1028 (1996).
- 329 18. A. G. Davies *et al.*, Atmospheric control of the cooling rate of impact melts and cryolavas on
330 Titan's surface. *Icarus* **208**, 887-895 (2010).
- 331 19. M. Hirzigtig *et al.*, Titan's surface and atmosphere from Cassini/VIMS data with updated
332 methane opacity. *Icarus* **226**, 470-486 (2013).
- 333 20. L. A. Soderblom *et al.*, Correlations between Cassini VIMS spectra and RADAR SAR
334 images: Implications for Titan's surface composition and the character of the Huygens probe
335 landing site. *Planet. Space Sci.* **55**, 2025–2036 (2007).

336 21. J. W. Barnes *et al.*, Spectroscopy, morphometry, and photoclinometry of Titan's dunefields
337 from Cassini/VIMS. *Icarus* **195**, 200-414 (2008).

338 22. R. N. Clark *et al.*, Detection and Mapping of Hydrocarbon Deposits on Titan. *J. Geophys.*
339 *Res.* **115**, E10005 (2010).

340 23. A. Le Gall *et al.*, Cassini SAR, radiometry, scatterometry and altimetry observations of
341 Titan's dune fields. *Icarus* **213**, 608-624 (2011).

342 24. L. E. Bonnefoy *et al.*, Compositional and spatial variations in Titan dune and interdune
343 regions from Cassini VIMS and RADAR. *Icarus* **270**, 222-237 (2016).

344 25. M. G. Tomasko *et al.*, A model of Titan's aerosols based on measurements made inside the
345 atmosphere. *Planet. Space Sci.* **56**, 669-707 (2008).

346 26. E. L. Barth and S. C. R. Rafkin, TRAMS: A new dynamic cloud model for Titan's methane
347 clouds. *Geophys. Res. Lett.* **34**, L03203 (2007).

348 27. E. L. Barth and S. C. R. Rafkin, Convective cloud heights as a diagnostic for methane
349 environment on Titan. *Icarus* **206**, 467-484 (2010).

350 28. K. R. Atkinson *et al.*, Penetrometry of granular and moist planetary surface materials:
351 Application to the Huygens landing site on Titan. *Icarus* **210**, 843-851 (2010).

352 29. S. E. Schroeder, E. Karkoschka, R. D. Lorenz, Bouncing on Titan: Motion of the Huygens
353 Probe in the seconds after landing. *Planet. Space Sci.* **73**, 327-340 (2012).

354 30. R. D. Lorenz, Wake-Induced dust cloud formation following impact of planetary landers.
355 *Icarus* **101**, 165-167, (1993).

356 31. R. Greeley, J. D. Iversen, Wind as a Geological Process on Earth, Mars, Venus, and Titan
357 (Cambridge University Press, 1985).

358 32. Y. P. Shao, H. Lu, A simple expression for wind erosion threshold friction velocity. *J.*
359 *Geophys. Res.* **105**, 22437–22443 (2000).

360 33. P. Claudin, B. Andreotti, A scaling law for aeolian dunes on Mars, Venus, Earth, and for
361 subaqueous ripples. *Earth Planet. Sci. Lett.* **252**, 30–44 (2006).

362 34. J. F. Kok, E. J. R. Parteli, T. I. Michaels, D. B. Karam, The physics of wind-blown sand and
363 dust. *Rep. Prof. Phys.* **75**, 106901 (2012).

364 35. J. W. Barnes *et al.*, Production and global transport of Titan’s sand particles. *Planet. Sci.* **4**, 1
365 (2015).

366 36. R. Sullivan *et al.*, Wind-driven particle mobility on Mars: Insights from Mars Exploration
367 Rover observations at “El Dorado” and surroundings at Gusev Crater. *J. Geophys. Res.* **113**,
368 E06S07 (2008).

369 37. T. Tokano, Relevance of fast westerlies at equinox for eastward elongation of Titan's dunes.
370 *Aeolian Res.* **2**, 113–127 (2010).

371 38. B. Charnay *et al.*, Methane storms as a driver of Titan’s dune orientation. *Nature Geosci.* **8**,
372 362–366 (2015).

373 39. S. C. R. Rafkin and E. L. Barth, Environmental control of deep convective clouds on Titan:
374 The combined effect of CAPE and wind shear on storm dynamics, morphology, and lifetime. *J.*
375 *Geophys. Res. Planets* **120**, 739–759 (2015).

376 40. D. M. Burr *et al.*, Higher-than-predicted saltation threshold wind speeds on Titan. *Nature*
377 **517**, 60–63 (2015).

378

379 **Supplementary Information** is linked to the online version of the paper at
380 www.nature.com/nature.

381

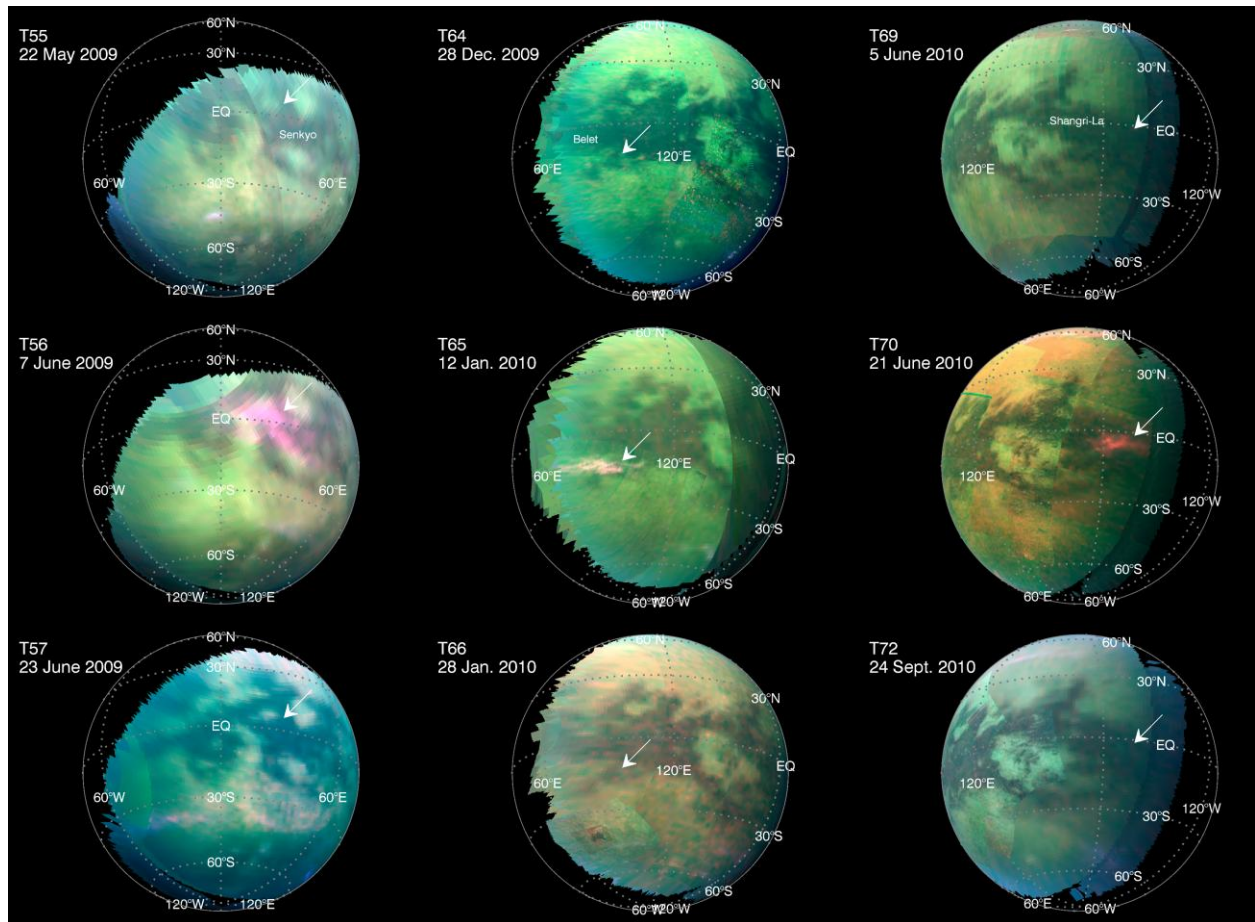
382 **Acknowledgments** We wish to thank P. Claudin and B. Andreotti for helpful discussions,
383 especially regarding thresholds and modes of sediment transport. We are also deeply grateful to
384 the Cassini/VIMS team for the calibration and planning of the data. We acknowledge financial
385 support from the UnivEarthS LabEx program of Sorbonne Paris Cité (ANR-10-LABX-0023 and
386 ANR-11-IDEX-0005-02), the French National Research Agency (ANR-APOSTIC-11-BS56-002
387 and ANR-12-BS05-001-03/EXO-DUNES) and the CNES. This study was partly supported by
388 the Institut Universitaire de France. TC was funded by the ESA Research Fellowship Programme
389 in Space Sciences. Part of this work has been performed at the Jet Propulsion Laboratory,
390 California Institute of Technology under contract with NASA.

391

392 **Author Contributions** S.R., S.L.M., J.W.B., J.B and G.V. discovered the brightening spots in
393 the VIMS dataset and first emitted the dust storm hypothesis. S.R., T.A., M.H., L.M., P.R.,
394 C.A.G. and A.C. developed, adapted, ran the radiative transfer model and designed the inversion
395 scheme including a low atmospheric layer of suspended particles. B.C., J.F.K., R.D.L., J.R., C.N.
396 and S.C.P. helped with the wind and sediment transport calculations. J.F.K., C.N., T.C., O.B.,
397 and A.L. participated to the discussion of the geological implications of dust storms occurrence
398 in Titan's atmosphere. C.S., R.H.B., K.H.B., B.J.B., R.N.C. and P.D.N. designed the planning of
399 VIMS observations. S.R. drafted the manuscript with contributions from all authors.

400

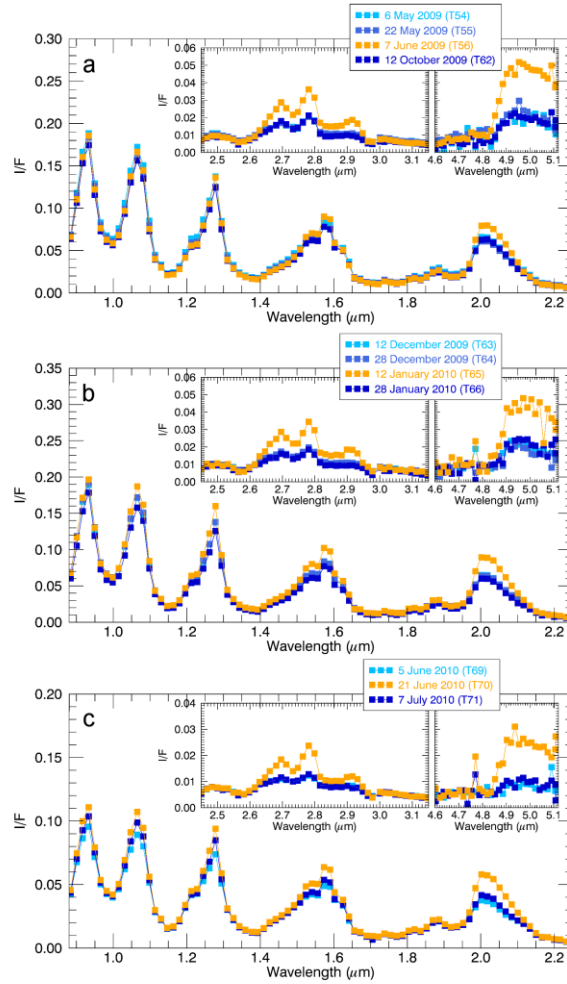
401 **Author Information** Reprints and permissions information is available at
402 www.nature.com/reprints. Correspondence and requests for materials should be addressed to
403 S.R. (rodriguez@ipgp.fr).



404
 405 **Fig. 1. VIMS color composite maps of Titan's singular brightening events that occurred in**
 406 **June 2009 (T56 flyby), January 2010 (T65) and June 2010 (T70).** Each column presents a
 407 time series showing VIMS Titan images (using the same RGB coding, red being the average
 408 between 5 and 5.07- μm , green being 2- μm and blue one being 2.78- μm) acquired over the same
 409 area just before (top), during (middle) and immediately after the brightening (bottom) for each
 410 individual event. White arrows designate the location of the infrared brightenings, centered at
 411 $\sim 24^\circ\text{E}$ and $\sim 2^\circ\text{S}$ (T56), $\sim 96^\circ\text{E}$ and $\sim 14^\circ\text{S}$ (T65), and $\sim 175^\circ\text{W}$ and $\sim 5^\circ\text{S}$ (T70) and covering a
 412 large fraction of the Senkyo, Belet and Shangri-La sand seas respectively (see also **Fig. S1b**).

413

414



415

416 **Fig. 2. VIMS infrared spectra of the brightening events that occurred at T56, T65 and T70**

417 **flybys. (a)** The gold squares represent the infrared spectrum extracted from the brightest pixel in

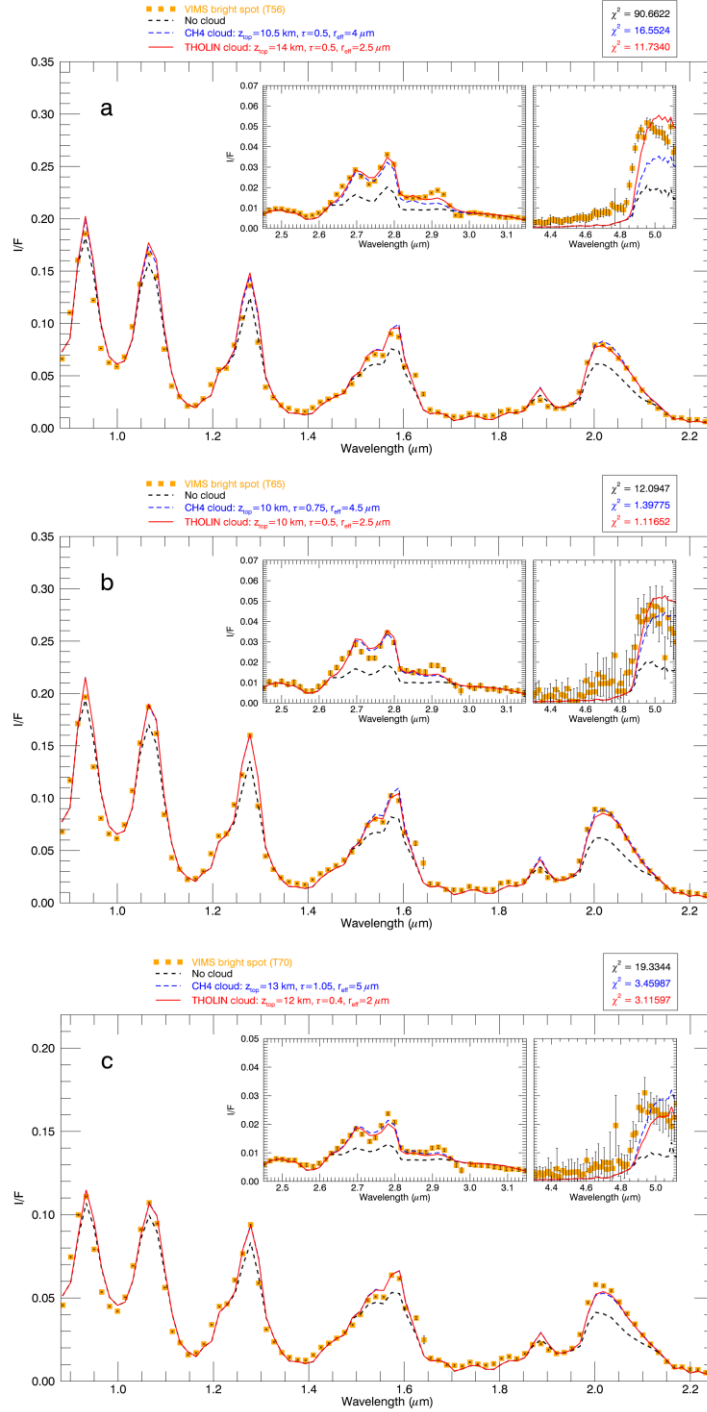
418 the central region of the brightening regions shown in **Fig. 1** for T56. This spectrum is compared

419 with those extracted from the same location from flybys as close in time as possible, before and

420 after the brightening event (blue tone squares). Same for T65 **(b)** and T70 **(c)**.

421

422



423

424 **Fig. 3. Observed spectra of the brightest pixels of the T56 (a), T65 (b) and T70 (c) bright**

425 **spots are compared with best-match calculated spectra.** The observed infrared spectra are

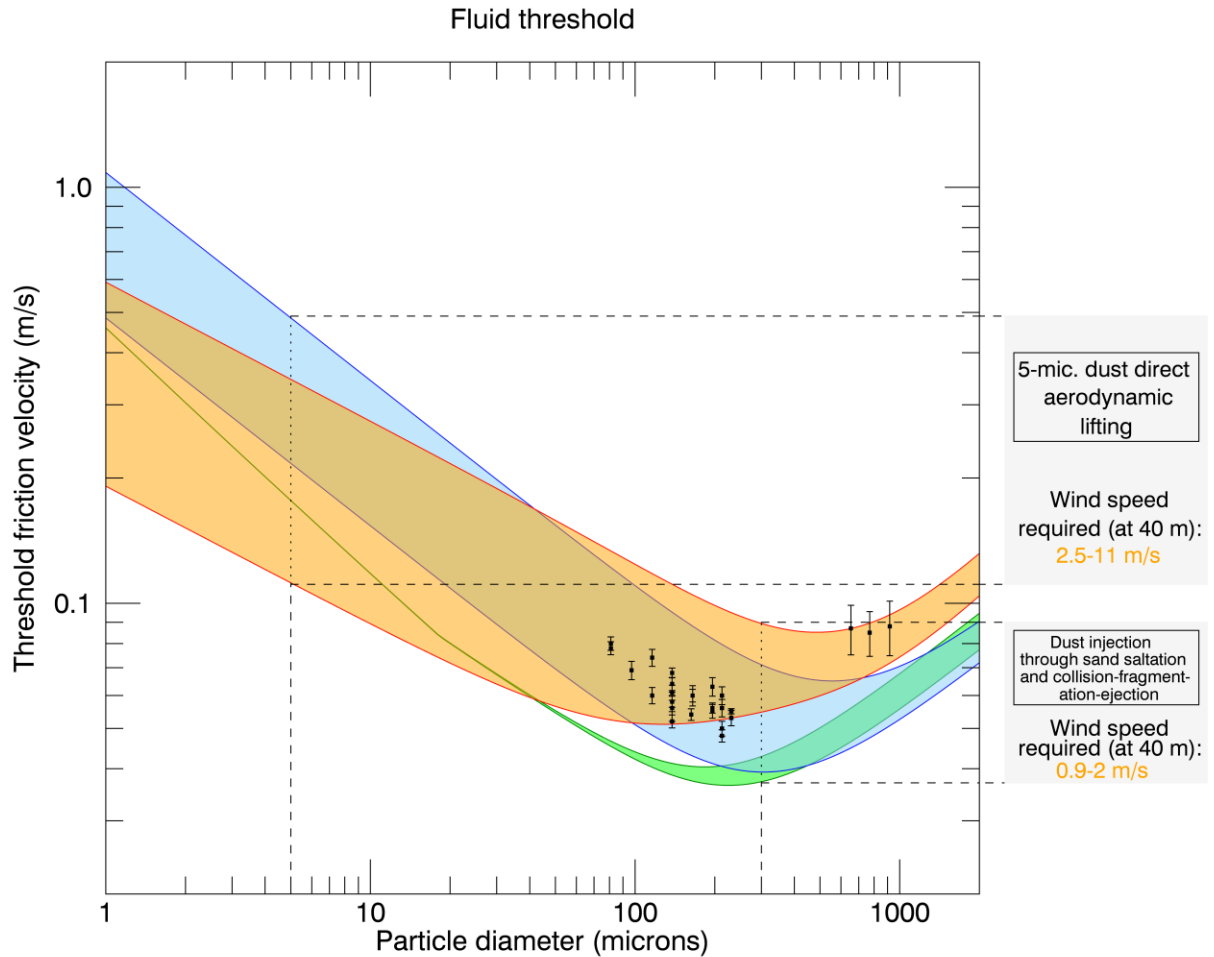
426 shown in yellow squares (identical to the yellow spectra shown in **Fig. 2**), along with their 1σ

427 error bars calculated from the VIMS signal-to-noise ratio. We modelled spectra with no cloud

428 contribution (black dashed curves), with no satisfactory agreement with the observations. In all
429 cases, the addition of a low altitude cloud composed of solid organic particles (red curves)
430 provides the best fits over the full VIMS wavelength range. Despite systematic poorer fits, best
431 fits for liquid methane clouds are also shown (blue dashed curves). Reduced χ^2 are indicated for
432 the “surface-only”, liquid methane and solid organic cloud models, along with the best retrieved
433 parameters for the two kinds of clouds (**Table S5**).

434

435



436
 437 **Fig. 4. Transport thresholds on Titan.** Intervals of friction velocity at the fluid threshold
 438 computed from formulae given in ref. (31) (green area), ref. (32) (blue area) and ref. (33) (orange
 439 area) for a range of possible mass densities ($800\text{-}1200\text{ kg}\cdot\text{m}^{-3}$) and interparticle forces ($\gamma = 1\text{-}$
 440 $5\cdot 10^{-4}\text{ N/m}$) for Titan's surface material³² (see **Table S6**). The calculated threshold curves are in
 441 very good agreement with recent wind-tunnel measurements under Titan's atmospheric and
 442 sedimentary conditions⁴⁰ (black squares with error bars). Range of needed near-surface wind
 443 speeds are given for 5-microns dust direct aerodynamic lifting and dust injection through
 444 saltation and collision-fragmentation-ejection processes respectively.

445